VORTEX INDUCED VIBRATIONS IN TWO DIRECTIONS (2D VIV)

AS6050: Dynamic Fluid Structure Interaction

Submitted By,

Achu Shankar
AE16B102
Department of Aerospace Engineering
IIT Madras

1.Introduction

Vortex Induced Vibration is a common phenomenon encountered in processes where a fluid interacts with a bluff solid structure. The of understanding the physics driving the phenomenon is of great significance for engineering applications. VIV is of critical concern both technically as well as economically for design of cylindrical offshore structures, pipelines and various other situations where a bluff body meets a flowing fluid. The oscillations due to VIV has shown to result in fatigue and further failure of structures. Recent studies have shown that the phenomenon could also be used for harvesting power from a flowing fluid (Guilherme R. Franzini, 2018). Even though the basic understanding of the underlying physics have been extensively investigated and the mechanism well known, a reliable mathematical model for predicting the associated fluid–structure interaction and nonlinear dynamical behavior is still under active research.

VIV occurrences are generally classified as crossflow or in-line VIV, in which the structure oscillates transverse to or aligned to the flow direction. Even though generally VIV is a 2D phenomenon having both the cross flow and in-line component, many studies have focused only on modelling the cross flow component, due to the lift force, as the amplitude response is larger compared to the in-line component. Several experimental studies have pointed out the significant effects of the in-line motion. The in-line motion is seen to contribute as much as the cross flow to current induced fatigue. Flow visualizations have also illustrated different vortex mode patterns in the wake behind cylinder oscillating with 1-DOF vs 2-DOF. Also due to the fact that many structures have different natural frequencies in different directions, a condition of coupled cross flow and in-line VIV can occur and lead to dangerously amplified dynamics.

Several researches have applied phenomenological models with the lift forces described by a van der pol oscillator and the structural oscillation with a linear damped oscillator. One major draw back of such models is the assumption of linearity in the structural oscillator as non-linearity in the problem can give raise to a lot of new phenomenon. Recently (Narakorn Srinil, 2012) has proposed a new model for 2D VIV which uses a double Duffing–VanderPol(structural-wake) oscillator. This model has been able to capture important aspects of 2D VIV and has shown agreement with various experimental data. In this project the vortex induced virations in two dimensions is studied using this model. Comparisons with experimental results are done whenever data exist for the described case.

2. Two Dimensional VIV Model

Figure 1 shows a schematic model of a cylinder undergoing cross flow/in-line VIV. Equations.[(1)-(4)] represents the model proposed by (Narakorn Srinil, 2012). The four equations model the structural and aerodynamic force oscillations in the in-line and cross-flow directions respectively.

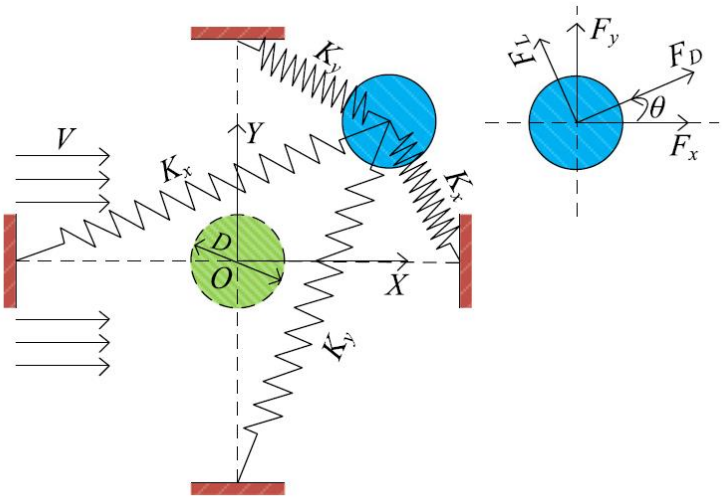

Figure 1:Schematic diagram of a flexibly mounted circular cylinder undergoing in-line and cross-flow oscillations, taken from (Narakorn Srinil, 2012)

$$\ddot{x} + \lambda_x \dot{x} + f^*(x + \alpha_x x^3 + \beta_x x y^2) = M_D \Omega^2 p + 2\pi M_L \Omega^2 \left(\frac{q\dot{y}}{V_r}\right) \quad (1)$$

$$\ddot{p} + 2\varepsilon_x \Omega (p^2 - 1)\dot{p} + 4\Omega^2 p = \Lambda_x \ddot{x} \quad (2)$$

$$\ddot{y} + \lambda_y \dot{y} + y + \alpha_y y^3 + \beta_y y x^2 = M_L \Omega^2 - 2\pi M_D \Omega^2 \left(\frac{p\dot{y}}{V_r}\right) \quad (3)$$

$$\ddot{q} + \varepsilon_y \Omega (q^2 - 1)\dot{q} + \Omega^2 q = \Lambda_y \ddot{y} \quad (4)$$

Where the dimensionless length units x and y given by x=X/D and y=Y/D, lift and drag components $p = 2\frac{C_D}{C_{D0}}$, $q = 2\frac{C_L}{C_{L0}}$ in which C_{D0} and C_{L0} are associated drag and lift for a stationary cylinder (assumed to be C_{D0}= 0.2, C_{L0}= 0.3), $\Omega = St\, V_r$ represents the ratio of vortex-shedding frequency to the cylinder cross-flow natural frequency in still water. The amplitude in in-line and cross-flow are represented in the graphs using A_x/D and A_y/D respectively.

MD and ML are the system mass parameters defined as,

$$M_D = \frac{C_{D0}}{16\pi^2 St^2 \mu} \qquad M_L = \frac{C_{L0}}{16\pi^2 St^2 \mu}$$

In which μ is given by ,

$$\mu = \frac{m_5 + m_f}{\rho D^2}$$

The damping terms $\lambda_x$and λ_y which account for both structural and fluid damping are given by,

$$\lambda_x = 2\xi_x f^* + \gamma\Omega/\mu_x \ , \quad \lambda_y = 2\xi_y + \gamma\Omega/\mu_y$$

mass ratio m^* is expressed as

$$m^* = \frac{4\mu}{\pi} - C_M$$

Also for ϵ_y an empirical formula derived from experimental data is used,

$$\epsilon_y = 0.00234e^{0.228m^*}$$

In all the further cases considered, m^* is taken as same in both x and y directions and damping ratio $\xi_x = \xi_y = \xi$ is also taken to be equal unless specified. Finally $\alpha_x, \alpha_y, \beta_x$ and β_y are dimensionless geometric parameters and are taken to be $\alpha_x = \alpha_y = \beta_x = \beta_y = 0.7$, $\Lambda_x = \Lambda_y = 12$, $\epsilon_x = 0.3$ unless specified.

Some peculiar aspects of this model compared to previous models are inclusion of the terms,(x^3, xy^2, y^3, x^2y) and $(q\dot{y}, p\dot{y})$, where the former set captures the axial stretching /structural coupling of x-y displacements and latter allowing the wake-cylinder interactions considering the relative velocity of the cylinder and the incoming flow .

The nonlinear Eqn.[(1)-(4)] were numerically solver using a fourth order four step Runge-Kutta scheme with a time step of 0.001 and initial conditions at $t = 0$ of $x = y = 0, p = q = 2$ and zero velocities. Most cases involve finding the response of the system with varying V_r . In all simulations V_r is varied in steps of 0.1 .

3.Results

In this section the results obtained from a detailed study done on the model is presented. Experimental values are also compared wherever it was available .

3.1 Effect of damping ratio

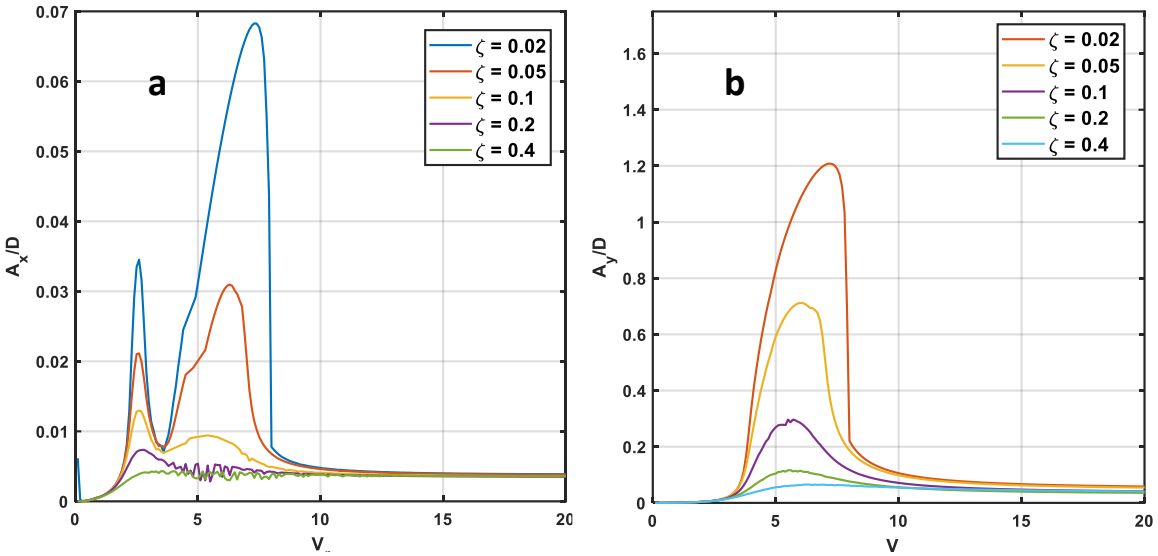

Figure 2: comparison of effect of damping ratio on variation of max amplitude of (a) in-line and (b) cross-flow directions with $m^* = 5.4$ and $f^* = 1$

First the case of varying damping ratio is considered. In this case all the other parameter are fixed namely $m^* = 5.4$ *and* $f^* = 1$. Figure 1 shows the variation of max value of cross-flow and in-line amplitudes with reduces velocity. It can be clearly seen that the max amplitude in the lock in regions increase as the damping ratio decreases for both in-line and cross-flow components. But the change in damping ratio is seen to have minimal effect in the lock-in region this again is same of both the components. Another peculiar observation is that the sharp fall in amplitude with V_r increase seems

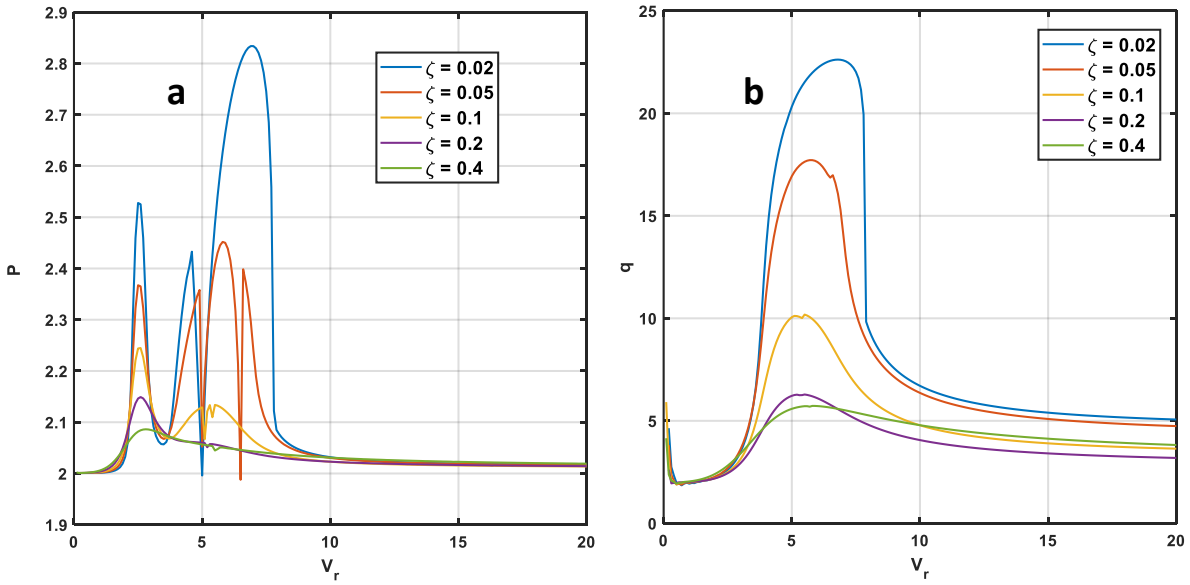

Figure 3: Effect of damping ratio on (a)drag and (b)lift components for $m^* = 5.4$ and $f^* = 1$

to vanish as the damping ratio increases and the transition from lock-in region to the other regions becomes more smooth. Compared to the cross-flow component the in-

line component is seen have relatively smaller amplitude which is as expected. Another interesting observation is the presence of a second smaller resonance region for the in-line component, this is a peculiar feature that has been observed in experiments as well.

Figure 2 shows the trends for the lift and drag components. Here also similar trends to that of cross-flow and in-line components respectively are observed. Similar ranges of V_r for lock-in as well as presence of a second resonance peak for drag is also seen.

The drag and the in-line component numerical results have some noise like features in them, these are suspected to be introduced due to some numerical error as they are more or less random.

3.2 Effect of mass ratio

Change in mass ratio has shown to have both qualitative and quantitative effects on the motion as well as the aerodynamic forces. Figure 3 shows the variation of the components of motion of the cylinder. A decrease in mass ratio shows an increase in the corresponding maximum amplitude in both the cross-flow as well as in-line motion.

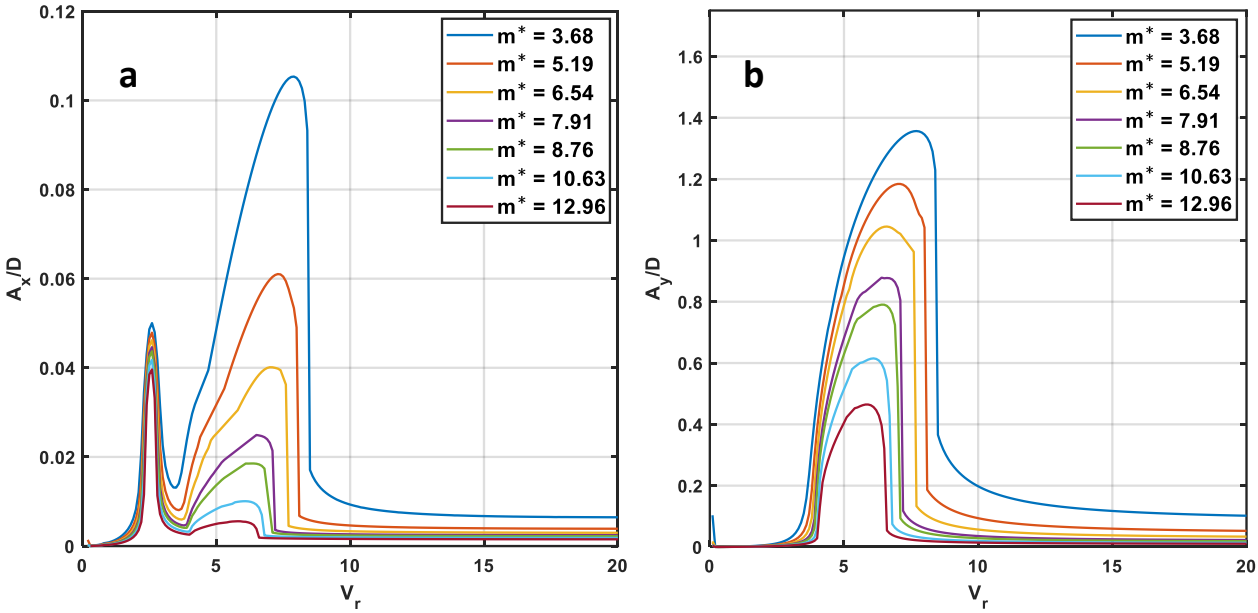

Figure 4: Effect of mass ratio variation on (a) in-line and (b)cross-flow components with $\xi_x = \xi_y = 0.006$ and $f^* = 1$

But in this case the lock-in range shows change with change in mass ratio. The lock-in range is seen to increase as the mass ratio decreases. Also here we can see that as the mass ratio increases the unlike in the case of varying damping the graph still maintains the sharp fall as mass ratio is increased. Here the second resonance peak for the in-line component is observed. Figure:4 shows the variations of the corresponding aerodynamic forces. Lift and drag show similar variations like the motion components like increase in amplitude and lock-in range with decrease in mass

ratio. For the numerical results obtained for drag shows noise this again is attributed to numerical errors.

Figure 5 and Figure 6 shows variation of only the in-line motion with varying mass ratio and damping ratiol respectively and compares the numerical results with experimental results from (Stappenbelt, 2007) and (Blevins, 2009) . For the varying mass ratio case we can see good agreement of the numerical and experimental results. The model is able to capture features like the lock-in range, sharp fall etc. For the case of varying damping the numerical results apart from a second resonance peak also predicts a third peak which is has the highest magnitude, this has phenomenon has been observed in some experiments as well.For this case the numerical and the experimental result have some deviation. This can be reduced by tuning the parameters in the model.

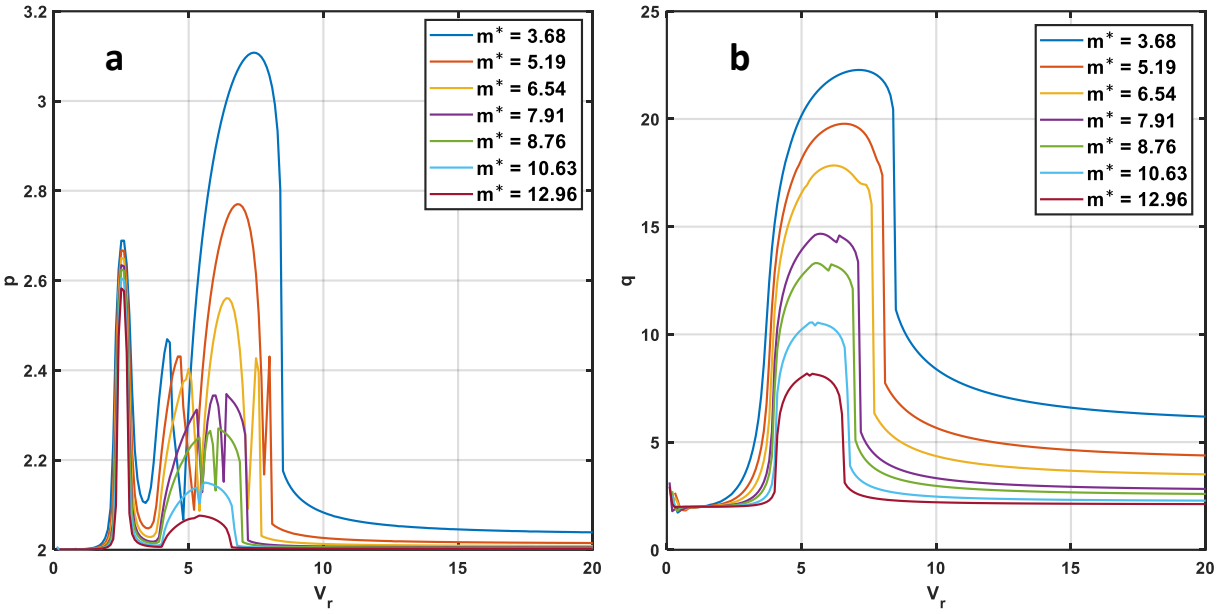

Figure 5: Effect of mass ratio on (a) drag and (b) lift components of aerodynamic forces with $\xi_x = \xi_y = 0.006$ and $f^* = 1$

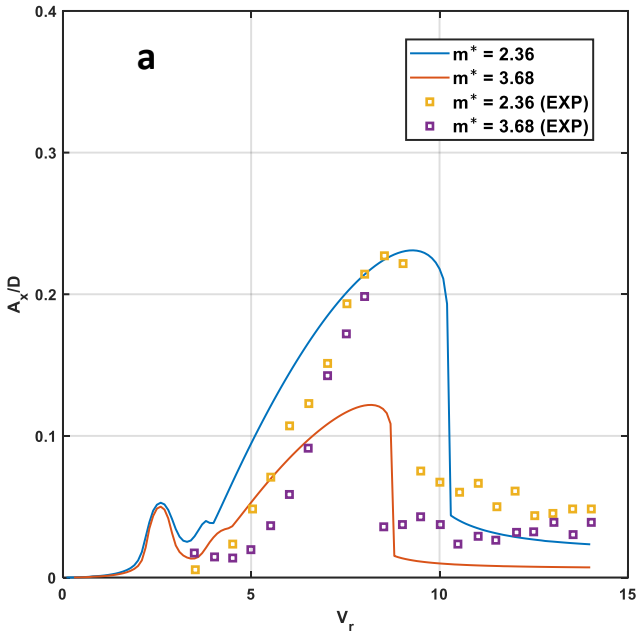

Figure 7: Effect of mass ratio on in-line motion numerical and experimental comparison $\xi_x = \xi_y = 0.006$ and $f^* = 1$

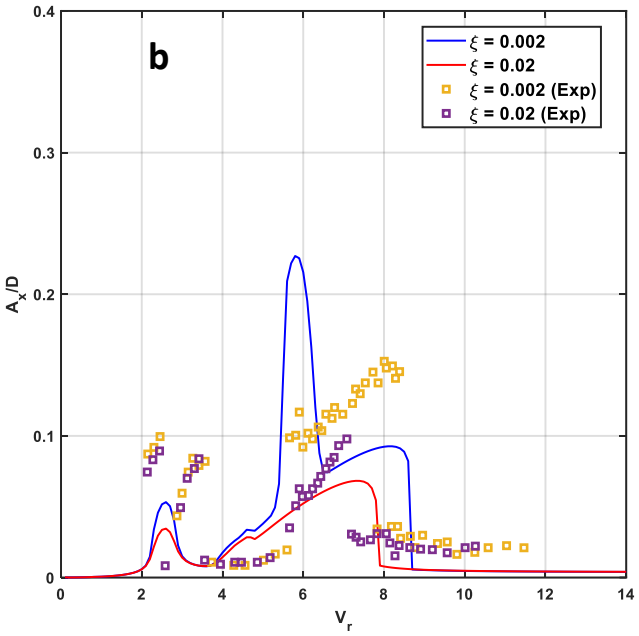

Figure 7: Effect of damping ratio on in-line motion , numerical and experimental comparison , $m^* = 5.4$ and $f^* = 1$

3.3 Hystersis phenomenon

One important phenomenon seen in many VIV problems is hystersis. In this section the model is tested to see if it can capture the hysteris phenomenon.

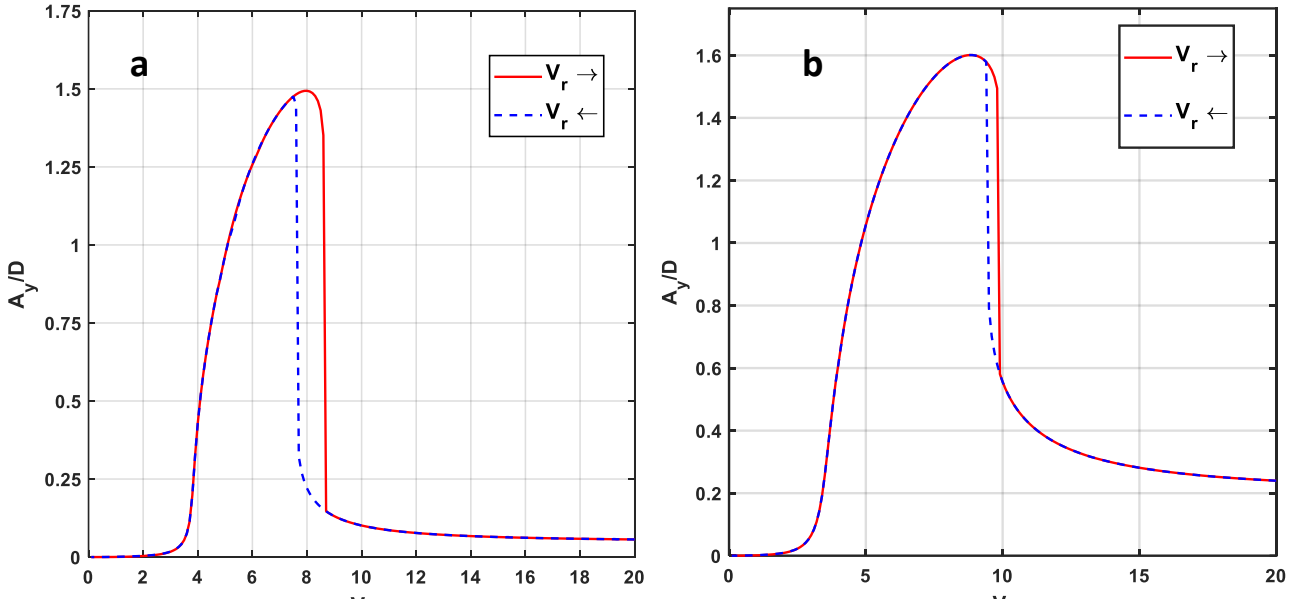

Figure 8: Cross-flow response(numerical) with increasing and decreasing V_r (a) $m^* = 5.4$, $\xi_x = \xi_y = 0.002, f^* = 1$ (b) $m^* = 2.36$, $\xi_x = \xi_y = 0.006, f^* = 1$

Figure:7 shows that the model is able to capture hysteresis phenomenon. It can be clearly seen that the sharp fall in amplitude occurs at different V_r values as you progress the simulation by increasing the V_r and by decreasing V_r. Comparing the two plots in Figure 7 we can see that the area of the hysteresis loop decreases as the product of mass ratio and damping ratio($m^*\xi$) increases. Figure 8 shows the trajectory the cylinder

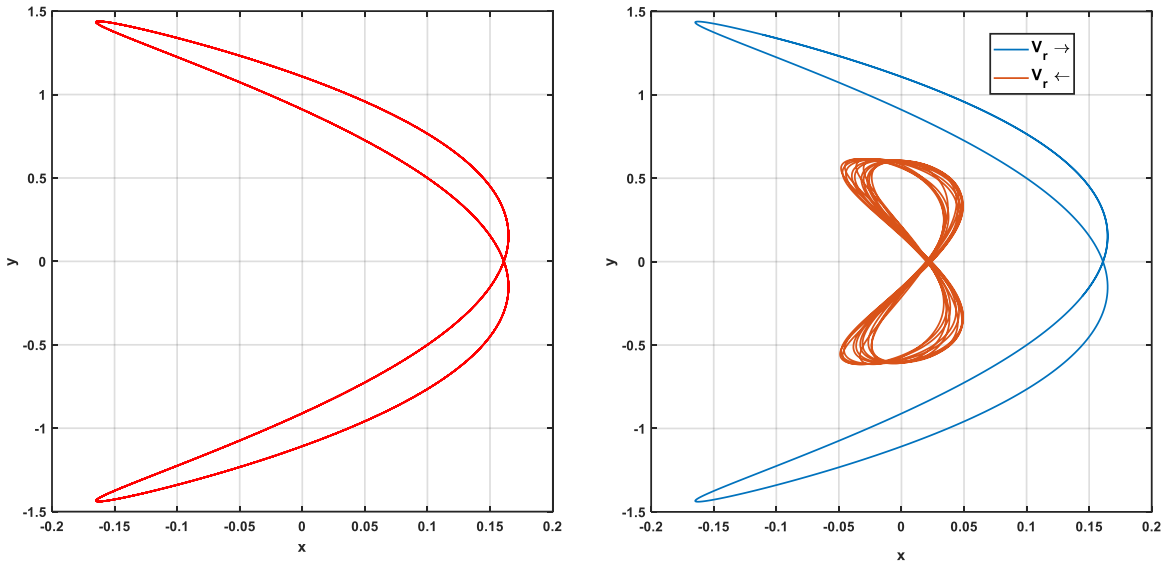

Figure 9: The trajectory of the cylinder with $m^* = 2.36$, $\xi_x = \xi_y = 0.006$, $f^* = 1$ at (a) $V_r = 8$ and (b) $V_r = 9.45$

takes when at $V_r = 8$ and $V_r = 9$ as you simulate in the increasing and decreasing direction of V_r. One interesting observation is that the trajectory obtained while running the simulation in the decreasing direction of V_r is show a something like a chaotic behavior, the occurrences of such behavior is not exactly known whether it is something that the model has introduced or is an inherent trait of the physical system.

3.4 Influence of cylinder geometrical nonlinearities and natural frequency ratio

The influence of cylinder geometrical nonlinearities is first discussed based on the experimental data of (Stappenbelt, 2007) with $m^* = 2.36$ and $\xi = 0.006$. Figure 9 and 10 show the response of in-line (A_x/D) and cross-flow (A_y/D for $f^* = 1$ *and* $f^* = 2$ respectively. Four cases are considered for both cases, with $\alpha_x = \beta_x = \alpha_y = \beta_y = 0.7$ taken as the reference solution of the numerical results. The experimental results are only available for $f^* = 1$ case. The reference solution shows good agreement with the experimental data. These simulations show the significance of the non-linearity terms.

Considering the first cases where $f^* = 1$ *and* $\alpha_x = \beta_x = 0$ this shows that the in-line nonlinearity has more effect on A_x/D than on A_y/D where the amplitude for the former has significant decrease but in both the cases the bent to right and the sharp fall at the end of the lock-in region is retained. For the case $f^* = 1$ *and* $\alpha_y = \beta_y = 0$

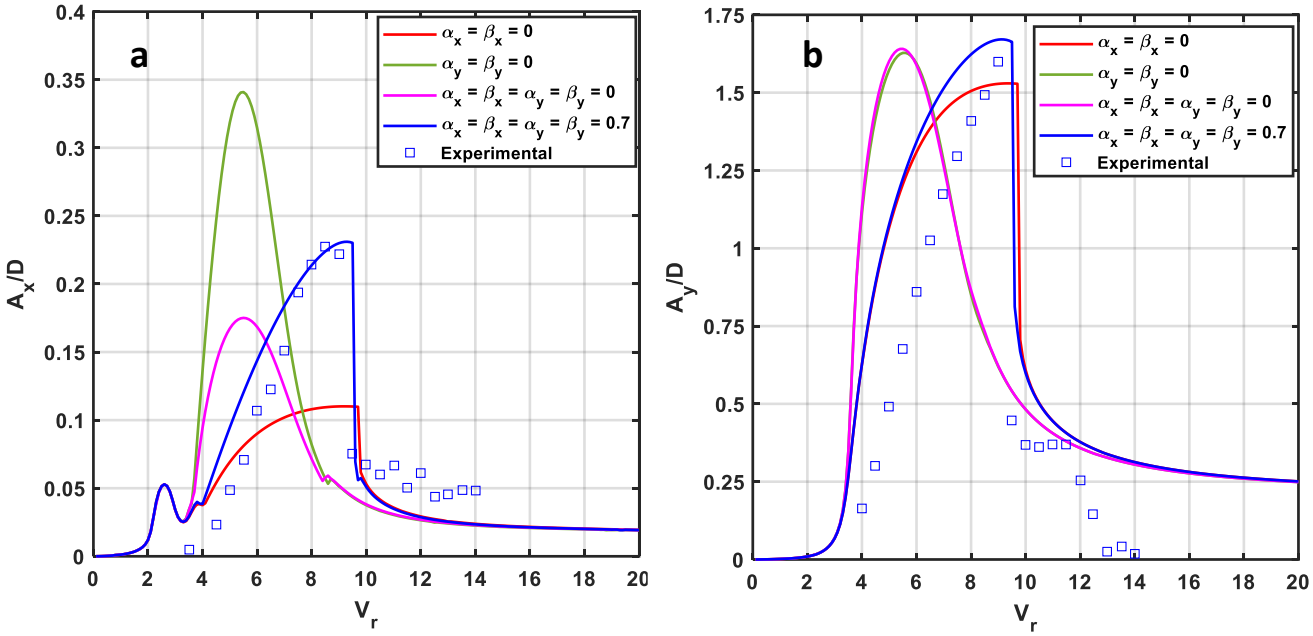

Figure 10: Effect of non-linearity on (a)in-line and (b) cross-flow amplitude for $m^* = 2.36$, $\xi = 0.006$, $f^* = 1$

here we can see both quantitative and qualitative changes for both motion components. For the in-line motion the amplitude has increased and has shifted to about $V_r = 5$, the lock-in region has reduced and the form of the plot has changed and has lost its bent to right and the sharp fall characteristics , for the cross-flow amplitude a slight decrease in the amplitude as well as shift in the peak is observed but the form of the plot has significant changes where the bent to right and sharp fall characteristics are also lost. For the case $f^* = 1$ *and* $\alpha_x = \beta_x = \alpha_y = \beta_y = 0$ the cross-flow shows similar behaviour to the previous case but the in-line component shows decrease in amplitude as well.

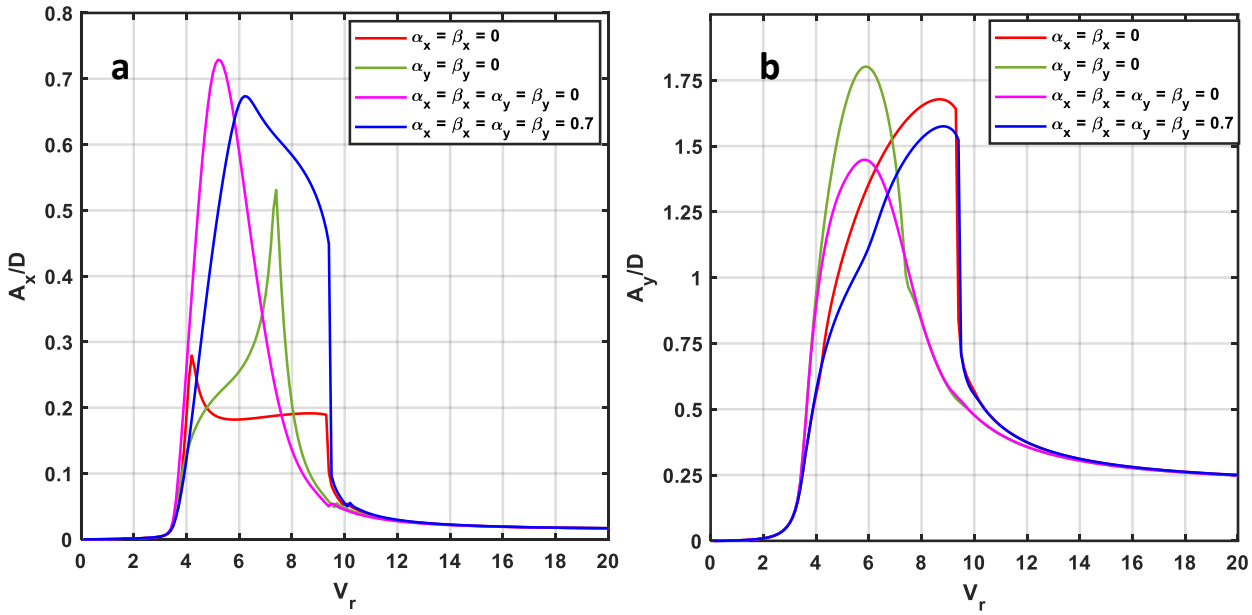

Figure 11 :Effect of non-linearity on (a)in-line and (b) cross-flow amplitude for $m^* = 2.36$, $\xi = 0.006$, $f^* = 2$

With $f^* = 2$ both the in-line and cross-flow nonlinearities now play a significant role in both A_x/D and A_y/D . Some important observations being, for the $f^* = 1$ case there was a second resonance peak for A_x/D which is not observed in $f^* = 2$ case, the geometry of the plots for A_x/D for $f^* = 2$ case shows a significant change to the corresponding case when $f^* = 1$, the maximum value for A_y/D now occurs when $\alpha_x = \beta_x = 0$ and for A_x/D when $\alpha_x = \beta_x = \alpha_y = \beta_y = 0$. Also, the maximum amplitude is seen to be more for $f^* = 2$ than $f^* = 1$. Overall, the results show how omitting the non-linearities can significantly affect the prediction of both in-line and cross-flow components, depending also on the specified f^*.

3.5 Influence of wake–cylinder coupling

The effect the wake-cylinder coupling term was investigated and compared with experimental data from (Stappenbelt, 2007) with $m^* = 2.36$, $\xi = 0.006$, $f^* = 1$. Figure 11 shows the effect of individually varying Λ_x *and* Λ_y .By comparing experimental data $\Lambda_x = \Lambda_y = 12$ is seen to give the best results and is taken as the reference numerical solution.

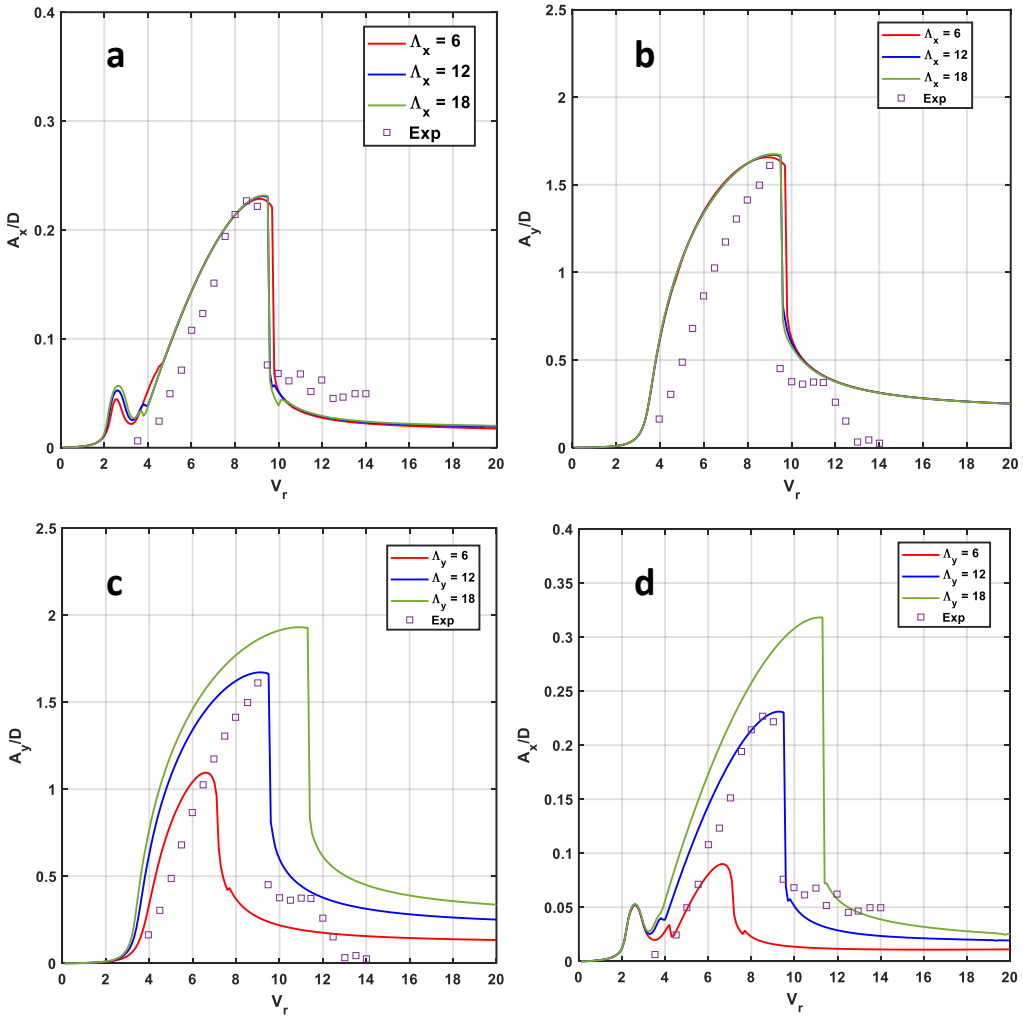

Figure 12:Comparison of numerical and experimental values for $m^* = 2.36$, $\xi = 0.006$, $f^* = 1$ by considering the effect of wake coupling terms.(a)in-line (b) cross-flow for varied Λ_x and .(c)in-line (d) cross-flow for varied Λ_y

Variation of Λ_x seems to have negligible effect in both in-line and cross-flow amplitudes as seen from the plots. On the contrary variation of Λ_y is seen to have large effects. Increasing Λ_y is seen to increase the maximum amplitude and widening of the lock-in range as well. From this it can be concluded that the cross-flow wake coupling term has more importance.

3.6 Influence of in-line wake coefficient

The overall effect of the in-line wake coefficient ϵ_x is seen to be minimal for both in-line and cross-flow amplitudes. For really small values of ϵ_x the peaks tends becomes more smooth and for the in-line component the amplitude of the second component is seen to increase as ϵ_x decreases. Overall, the results are not that sensitive to ϵ_x. Comparing the experimental data from (Stappenbelt, 2007) the best value of $\epsilon_x = 0.3$ is taken for all simulations with the model.

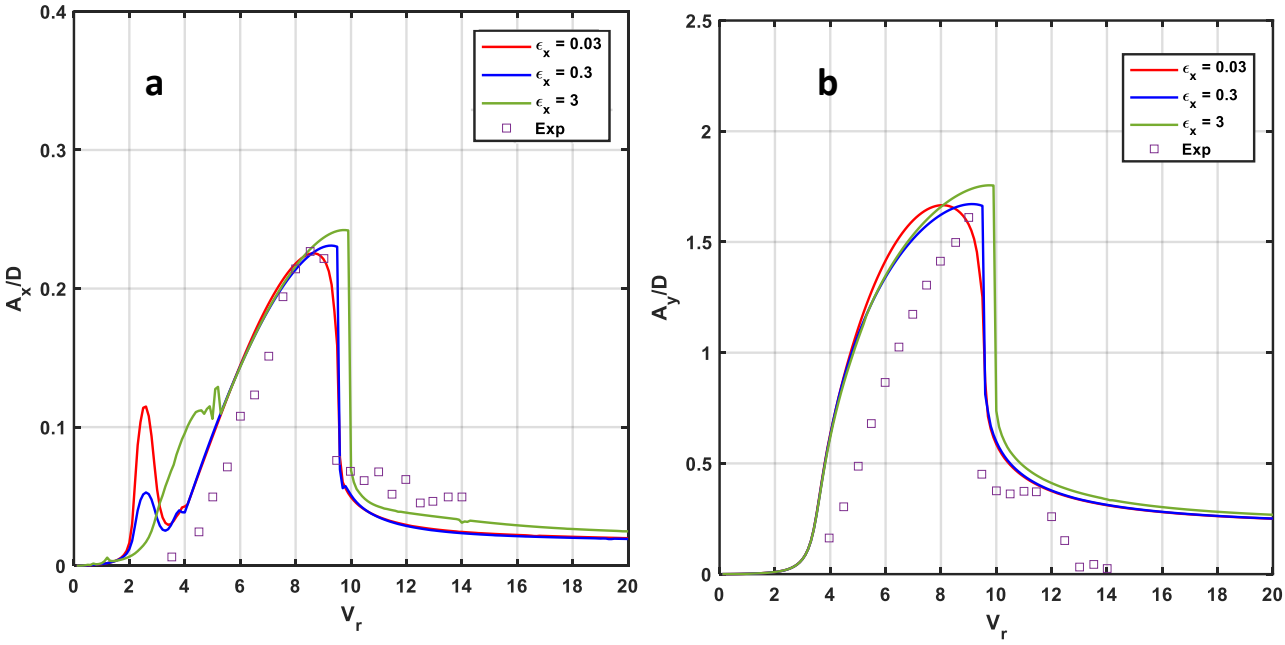

Figure 13:Effect of in-line wake coefficient on (a) in-line and (b)cross-flow maximum amplitude for $m^* = 2.36, \xi = 0.006, f^* = 1$

3.7 Influence of quadratic nonlinear terms

The relative velocity between the flow and cylinder is discarded which are reflected in the equation by the quadratic nonlinear terms in RHS of Eqn.(1) and (3). Figure 14 shows the trajectory solved with and without considering the quadratic nonlinear terms. We can clearly see both quantitative and qualitative differences between the cases the in-line amplitude reduces considerably and the figure of eight trajectory observed in experiments as well is not obtained without the inclusion of quadratic nonlinear terms. This highlights the fact that the characteristic figure of

eight and 2:1 resonance is associated with the quadratic nonlinear term, and neglecting it might lead to uncoupling between the in-line and cross-flow VIV response.

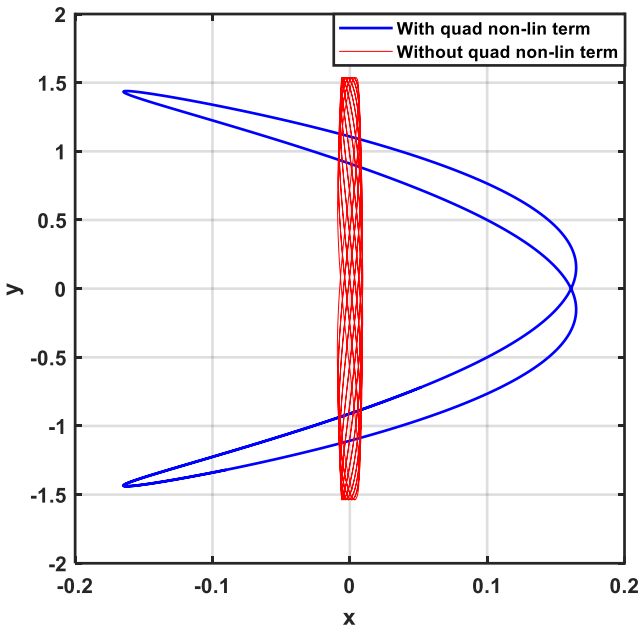

Figure 14:Effect of quadratic non-linear terms on the trajectory of cylinder with $m^* = 2.36\ , \xi = 0.006, f^* = 1$

3.8 Effect of strutural natural frequency ratio

The influence of f^* is illustrated in Figure 15 with $m^* = 5.4\ , \xi = 0.002$ for $f^* = 1, 1.2, 1.4, 1.6, 1.8, 2$. Simulations are ran for $V_r = 4.5\ , 6\ , 7, 7.6$. Regardless of f^* value t most of the trajectories are of figure-eight orbits. The variations between the trajectories are in their intial conditions, phase , in-line and cross flow amplitude etc. The trajectories for $V_r = 6, f^* = 1\ and\ V_r = 7.6, f^* = 1.2$ are not the figure-eight rather they are more towards being an ellipitcal orbit, recently such elliptical orbits have been found and explained to be due to a strong structural coupling by (Kheirkhah, 2012). Another obsevation is the large increase in amplitude for $f^* = 2$.

3.9 Comparison with KHL experimental data

Dataset	f_{ny} (Hz)	f_{nx} (Hz)	ξ_y (%)	ξ_x (%)	m_y^*	m_x^*	f^*
KHL1	0.312	0.316	1.0	4.7	1.4	1.4	1.01
KHL2	0.218	0.281	1.5	1.0	1.4	1.4	1.29
KHL3	0.262	0.419	1.6	1.0	1.4	1.4	1.60
KHL4	0.203	0.376	1.8	1.2	1.4	1.4	1.85
KHL5	0.192	0.192	2.0	3.1	1.4	1.4	1.00
KHL6	0.223	0.223	1.5	2.3	3.5	3.5	1.00

Table 1: The 2D VIV experimental data from Kelvin Hydrodynamics Laboratory (KHL) of the University of Strathclyde, Glasgow, UK

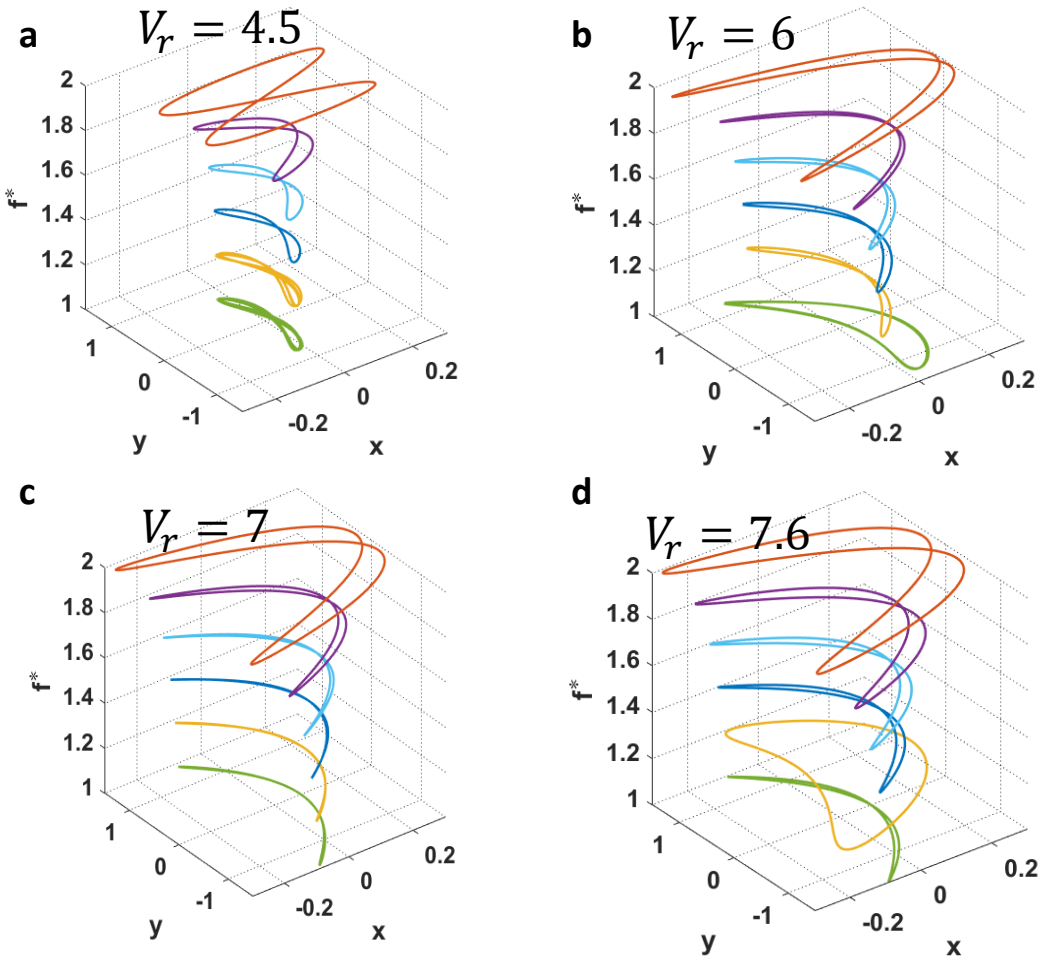

Figure 15: 2D trajectories with $m^* = 5.4$, $\xi = 0.002$, with various f^*: (a) $V_r = 4.5$ (b) $V_r = 6$ (c)$V_r = 7$ and, (d) $V_r = 7.6$

The VIV model was compared with experimental data obtained from the Kelvin Hydrodynamics Laboratory (KHL) of the University of Strathclyde, Glasgow, UK (NarakornSrinil n, 2013). These were a set of experiments conducted by researches who proposed the 2D VIV used in this project. Mainly two comparisons are made for different parameters namely a comparison of the amplitude response and of a frequency response.

Figure 16 shows the amplitude response for KHL 1 and KHL 4 the main difference between the two are f^* and damping ratios. Looking at the results we can see that the model is able to capture a lot of the qualitative behaviour of the system, with KHL 1 condition the cross-flow amplitude response predicted by the model agrees well with experimental data, but for the in-line response the maximum value from the numerical results are far less than the experimental values even though the Rms values are comparable. For the KHL 4 conditions the cross-flow and in-line response predicted by the model is higher than the experimental results.

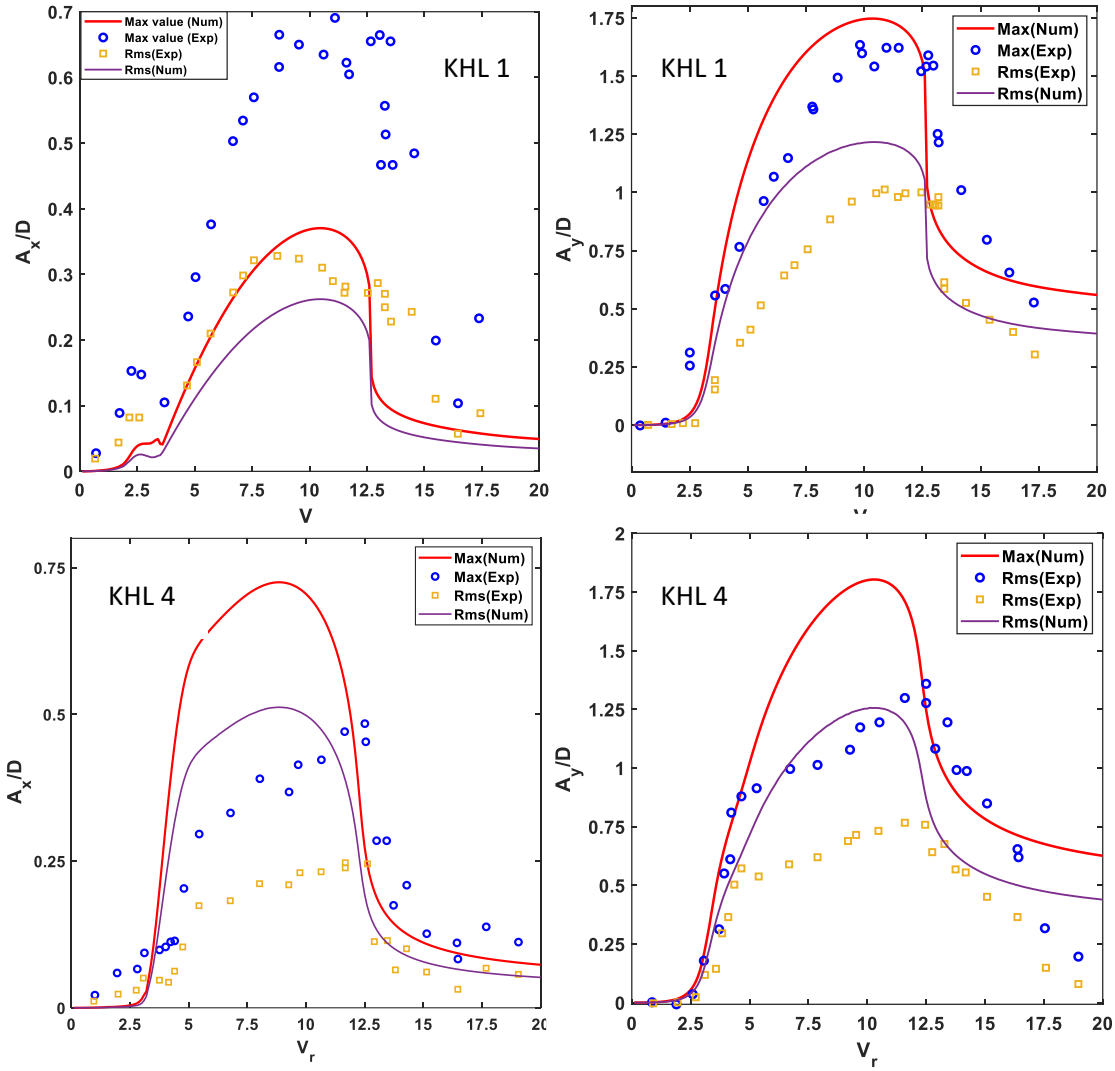

Figure 16: Comparison of numerical and experimental in-line and cross -flow maximum and Rms amplitude responses based on KHL data

Figure 17 shows the comparison of frequency response of numerical and experimental results for two KHL dataset . The numerical and experimental data shows good agreement with each other especially in the lock-in range. One peculiar observation in both the experimental and numerical results is the variation of frequency with reduced flow velocity being more like a straight line, this maybe due to the lower mass ratio of the cylinder.

4 Conclusion

The proposed model by (Narakorn Srinil, 2012) captures several fundamental VIV characteristics including 2D lock-in, hysteresis phenomena and figure-of-eight trajectories etc. These studies have shown the importance of in-line VIV component for the VIV problem. Certain remarks regarding the most important parameters for 2D VIV can be made from observations of the previous section. The behaviour of the system is independently governed by m*, ξ and f*. The results show a strong coupling

and interaction of cross-flow/in-line VIV motions takes place in the fluid-structure system with low m*, low ξ and f* = 2.

The cubic geometric non-linear term in the in-line equation has a quantitative effect on the in-line and cross-flow VIV response. Whereas the cubic geometric non-linear term in the cross-flow equation has both quantitative as well as qualitative effect on in-line and cross-flow response. Another conclusion that can be made is the fact that the quadratic non-linearities in the wake equations play a major role in the trajectories having figure of eight shape. The results also show the importance of tuning the empirical parameters of the model for it to actually capture real solutions.This model if properly calibrated is a vary useful tool to model the 2D VIV problem. In addition to be able to capture all the properties related to VIV in might be useful be able to reveal more insight into 2D VIV problems.

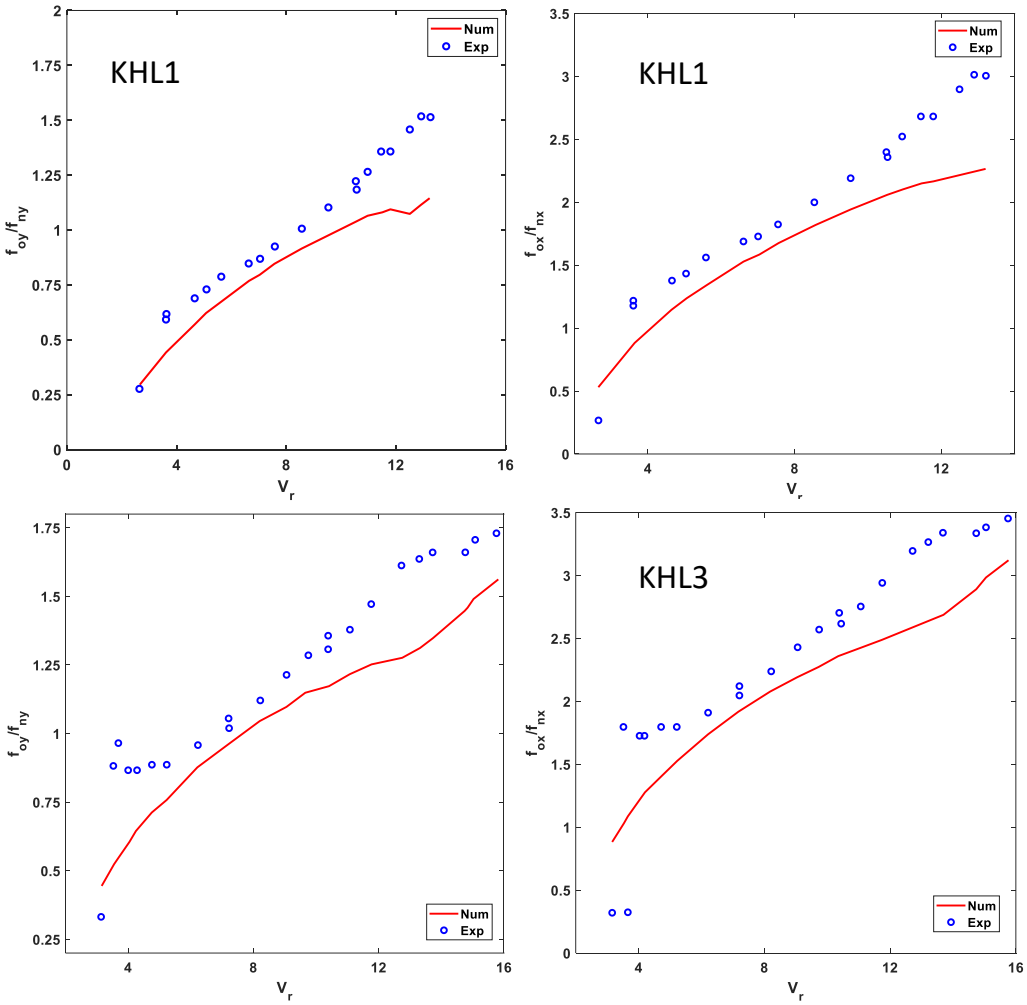

Figure 17: Comparison of numerical and experimental results of in-line and cross-flow oscillations for different KHL 1 and KHL 3 dataset.

References

Blevins, R. (2009). Experimental investigation of vortex-induced vibratiolns in one and two dimensions with variable mass, damping and Reynolds number . *Journal of Fluids Engineering* .

Guilherme R. Franzini, L. O. (2018). A numerical investigation on piezoelectric energy harvesting from Vortex-Induced Vibrations with one and two degrees of freedom. *Journal of Fluids and Structures*, 196-212.

Kheirkhah, S. (2012). Orbiting response in vortex-induced vibrations of a two-degree-of-freedom pivoted circular cylinder. *J.Fluids Struct*, 343-358.

Narakorn Srinil, H. (2012). Modelling ofcoupledcross-flow/in-linevortex-inducedvibrationsusing. *ELSEVIER Ocean Engineering*, 83-97.

NarakornSrinil n, H. (2013). Two-degree-of-freedom VIV of circular cylinder with variable natural frequency ratio:Experimental and numerical investigations. *Elsevier, Ocean Engineering*, 179-194.

Stappenbelt, B. (2007). Low mass ratio vortex-induced motion. *The 16th Australasian Fluid Mechanics Conference.*